Inorganic Chemistry
Cite This: Inorg. Chem. XXXX, XXX, XXX−XXX
Article
pubs.acs.org/IC

Mn(III)-Iodosylarene Porphyrins as an Active Oxidant in Oxidation Reactions: Synthesis, Characterization, and Reactivity Studies

Mian Guo,[†] Yong-Min Lee,[†] Mi Sook Seo,[†] Yong-Ju Kwon,[†] Xiao-Xi Li,[†] Takehiro Ohta,[‡] Won-Suk Kim,[†] Ritimukta Sarangi,*[,§] Shunichi Fukuzumi,*[,†] and Wonwoo Nam*[,†,¶]

[†]Department of Chemistry and Nano Science, Ewha Womans University, Seoul 03760, Korea
[‡]Picobiology Institute, Graduate School of Life Science, University of Hyogo, RSC-UH LP Center, Hyogo 679-5148, Japan
[§]Stanford Synchrotron Radiation Lightsource, SLAC National Accelerator Laboratory, Menlo Park, California 94025, United States
[¶]School of Chemistry and Chemical Engineering, Shaanxi Normal University, Xi'an 710119, People's Republic of China

Supporting Information

ABSTRACT: Mn(III)-iodosylarene porphyrin adducts, $[Mn(III)(ArIO)(Porp)]^+$, were synthesized by reacting electron-deficient Mn(III) porphyrin complexes with iodosylarene (ArIO) at −60 °C and characterized using various spectroscopic methods. The $[Mn(III)(ArIO)(Porp)]^+$ species were then investigated in the epoxidation of olefins under stoichiometric conditions. In the epoxidation of olefins by the Mn(III)-iodosylarene porphyrin species, epoxide was formed as the sole product with high chemoselectivities and stereoselectivities. For example, cyclohexene oxide was formed exclusively with trace amounts of allylic oxidation products; *cis*- and *trans*-stilbenes were oxidized to the corresponding *cis*- and *trans*-stilbene oxides, respectively. In the catalytic epoxidation of cyclohexene by an electron-deficient Mn(III) porphyrin complex and [s]PhIO at low temperature (e.g., −60 °C), the Mn(III)-iodosylarene porphyrin species was evidenced as the active oxidant that effects the olefin epoxidation to give epoxide as the product. However, at high temperature (e.g., 0 °C) or in the case of using an electron-rich manganese(III) porphyrin catalyst, allylic oxidation products, along with cyclohexene oxide, were yielded, indicating that the active oxidant(s) was not the Mn(III)-iodosylarene adduct but probably high-valent Mn-oxo species in the catalytic reactions. We also report the conversion of the Mn(III)-iodosylarene porphyrins to high-valent Mn-oxo porphyrins under various conditions, such as at high temperature, with electron-rich porphyrin ligand, and in the presence of base (OH^-). The present study reports the first example of spectroscopically well-characterized Mn(III)-iodosylarene porphyrin species being an active oxidant in the stoichiometric and catalytic oxidation reactions. Other aspects, such as one oxidant versus multiple oxidants debate, also were discussed.

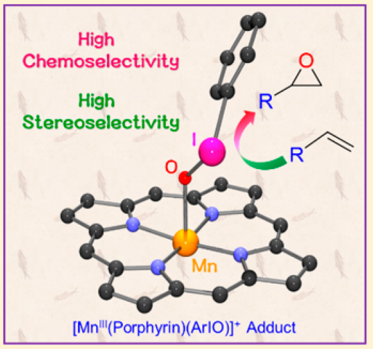

INTRODUCTION

Mechanistic elucidation of oxidation reactions catalyzed by transition-metal complexes has been the focus of current research in the communities of bioinorganic/biomimetic and oxidation chemistry, with the intention of developing efficient catalytic systems and understanding biologically important reactions mediated by metalloenzymes.[1,2] The mechanistic studies have been performed using artificial oxidants, such as iodosylarenes (ArIO), peracids, and H_2O_2, to generate metal−oxygen intermediates, and high-valent metal-oxo species have been proposed as the unique intermediates involved in the oxidation reactions by metalloenzymes and their model compounds.[3,4] However, there is mounting evidence supporting that multiple oxidants, such as metal-oxo and metal-oxidant adduct species, are involved in the oxidation reactions, and the mechanisms of the formation and oxidation reactions of the active oxidants are much more complex than initially proposed.[5,6]

Among the metal-oxidant adduct species, metal-iodosylarenes are one of the most intensively searched intermediates, since ArIO have been frequently employed as terminal oxidants in the synthesis of metal-oxo species, as well as in the catalytic oxidation of organic substrates.[7,8] However, only a few metal-iodosylarene complexes have been successfully synthesized and characterized spectroscopically and/or structurally, because of their thermal instability and fast conversion to the corresponding metal-oxo species.[9−12] For example, in heme and nonheme Mn systems, there is only one structurally characterized manganese-iodosylarene complex, which is a Mn(IV)-bis(iodosylbenzene) salen complex that was reported by Fujii and co-workers.[9] The only spectroscopically characterized mononuclear manganese-iodosylarene porphyrin adduct is a Mn(IV)-bis(iodosylbenzene) porphyrin complex.[10] Very recently, a Mn(III)-iodosylarene intermediate was trapped in catalytic reactions but with lack of full spectroscopic characterization and reactivity studies.[13] Herein, we report, for the first time, the synthesis and thorough spectroscopic

Received: May 25, 2018

DOI: 10.1021/acs.inorgchem.8b01426
Inorg. Chem. XXXX, XXX, XXX−XXX

characterization of mononuclear Mn(III)-iodosylarene porphyrin complexes (Scheme 1, reaction a). The adduct species

Scheme 1. Synthesis and Reactions of a Mn(III)-Iodosylarene Porphyrin Adduct (X = Cl^- or Solvent Molecule)

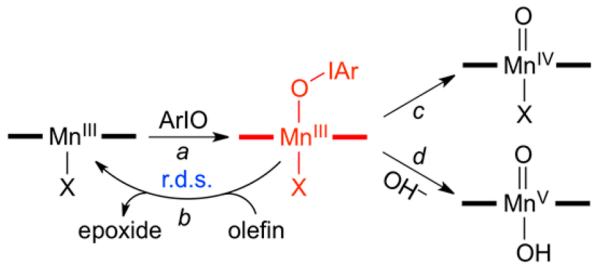

oxidize olefins to the corresponding epoxides with high chemoselectivities and stereoselectivities under stoichiometric and catalytic reactions (Scheme 1, reaction b). Mechanistic aspects for the conversion of the Mn(III)-iodosylarene adducts to the corresponding Mn-oxo complexes under various reaction conditions are also discussed in this study (Scheme 1, reactions c and d).

RESULTS AND DISCUSSION

Synthesis and Characterization of Mn(III)-Iodosylarene Porphyrins. The reaction of $[Mn^{III}(TDCPP)Cl]$[14] with 5 equiv of 1-(*tert*-butylsulfonyl)-2-iodosylbenzene (^{s}PhIO) in a solvent mixture of CH_2Cl_2/butyronitrile (BuCN)/CF_3CH_2OH (TFE) (v/v/v 5:5:1)[15] at −60 °C resulted in an immediate color change from brown to deep red, accompanied by a blue shift of the absorption band from 477 nm to 461 nm (Figure 1a). The formation of this species was extremely fast (within 300 ms), as monitored by a stopped-flow visible spectrophotometer (Figure 1a, inset). The new intermediate, denoted as **1**, with the Soret band at 461 nm and the Q-band at 560 nm, was sufficiently stable for spectroscopic characterization at −60 °C ($t_{1/2}$ ≈ 20 min) but decayed to the starting Mn(III)-(TDCPP) complex and Mn(IV)(O)(TDCPP) (**2**, vide infra) (see Figure S1a in the Supporting Information (SI)). The cold-spray ionization mass spectrum (CSI-MS) of **1** exhibited a prominent ion peak at a mass-to-charge ratio (m/z) of 1381.8, which corresponds to the mass and isotope distribution pattern of $[Mn(^sPhIO)(TDCPP)(CF_3CH_2O)]$ (calcd m/z = 1381.8) (Figure S2 in the SI). When the reaction was performed with ^{18}O-labeled ^{s}PhI^{18}O, the CSI-MS exhibited a peak at m/z = 1383.8 (Figure S2), which corresponds to $[Mn(^sPhI^{18}O)(TDCPP)(CF_3CH_2O)]$ (calcd m/z = 1383.8). The two-mass unit shift in the ^{18}O-labeled experiment suggests that **1** contains one molecule of ^{s}PhIO, which is further confirmed by EXAFS results (vide infra). The X-band EPR spectrum of **1** was silent (see Figure S3a in the SI). The resonance Raman (rRaman) spectrum of **1**, recorded at −60 °C upon 442 nm excitation, displayed one isotopically sensitive band at 699 cm^{-1}, which shifted to 661 cm^{-1} upon ^{18}O-substitution (Figure 1b). The observed isotopic shift of −38 cm^{-1} with ^{18}O-substitution is in good agreement with the calculated value for a diatomic I−O oscillator (−36 cm^{-1}). Note that I−O−Mn stretching bands of Mn(IV)-bis(iodosylbenzene) salen and Mn(IV)-bis(iodosylbenzene) porphyrin complexes were reported at ∼600 cm^{-1}.[9b,10]

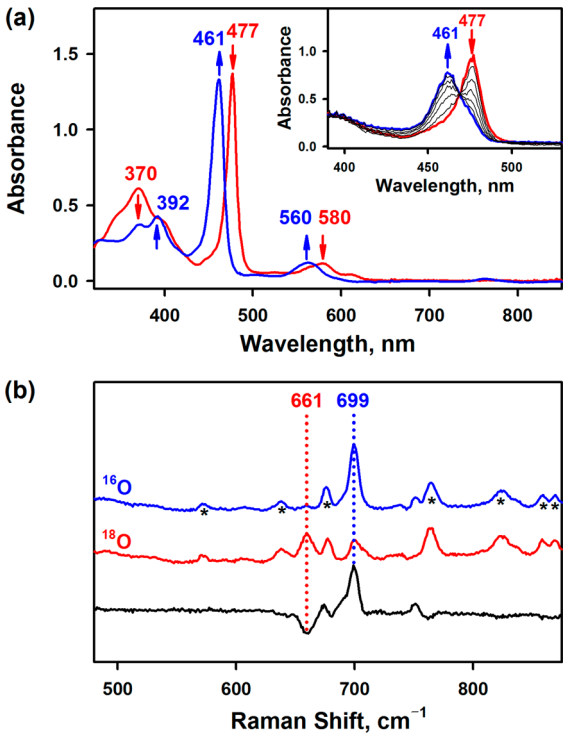

Figure 1. (a) Ultraviolet−visible light (UV-vis) spectral changes observed in the reaction of $[Mn^{III}(TDCPP)Cl]$ (0.10 mM, red line) and ^{s}PhIO (0.50 mM) to form **1** (blue line) in CH_2Cl_2/BuCN/TFE (v/v/v 5:5:1) at −60 °C. Inset shows visible spectral changes observed for the formation of **1** (blue line) from $[Mn^{III}(TDCPP)Cl]$ (0.075 mM, red line) and ^{s}PhIO (0.375 mM) at −60 °C by stopped-flow technique. The formation of **1** was complete within 300 ms. (b) Resonance Raman (rRaman) spectra of $[Mn^{III}(^sPhI^{16}O)(TDCPP)]^+$ (**1**-^{16}O, 2.0 mM; blue line) and $[Mn^{III}(^sPhI^{18}O)(TDCPP)]^+$ (**1**-^{18}O, 2.0 mM; red line) upon excitation at 442 nm at −60 °C. Black line is the difference spectrum of **1**-^{16}O and **1**-^{18}O. The peaks marked with asterisks originated from solvents.

Mn K-edge XAS and EXAFS measurements were performed on $[Mn^{III}(TDCPP)Cl]$ and **1** to determine the geometric structure and oxidation state of **1** (Figure 2a). A comparison of the Mn K-pre-edges, which arise due to Mn 1s → 3d electric dipole-forbidden, but quadrupole-allowed transition, is shown in the inset of Figure 2a. A slight decrease in pre-edge intensity in **1**, relative to $[Mn^{III}(TDCPP)Cl]$, is observed, indicating a more ordered first shell in **1**. More importantly, the pre-edges occur at very similar energies, indicating a rather insignificant change in ligand field strength and oxidation state.[16] A ∼1.5 eV blue-shift is observed in the rising-edge on going from $[Mn^{III}(TDCPP)Cl]$ to **1**, which is indicative of the loss of a heavier ligand (i.e., the Cl^- ligand in $[Mn^{III}(TDCPP)Cl]$) for a light-atom ligand (i.e., attributable to a ^{s}PhIO ligand).[17,18] To obtain structural information, FEFF analysis was performed on Mn K-edge EXAFS data for $[Mn^{III}(TDCPP)Cl]$ and **1** (Figure 2b), showing a comparison of the non-phase-shift-corrected Fourier transform (FT) data for the two species (the EXAFS comparison is shown in the inset). The data for **1** reveal an increase in the first-shell intensity, indicating increase in light-atom coordination at the Mn center. The loss of FT intensity at ∼2 Å in **1** indicates the loss/weakening of the Cl^- ligand. Both of the species have strong multiple-scattering contributions from the porphyrin ligand requiring long-range contributions in the FEFF fits. FEFF best fits to the data for

DOI: 10.1021/acs.inorgchem.8b01426
Inorg. Chem. XXXX, XXX, XXX−XXX

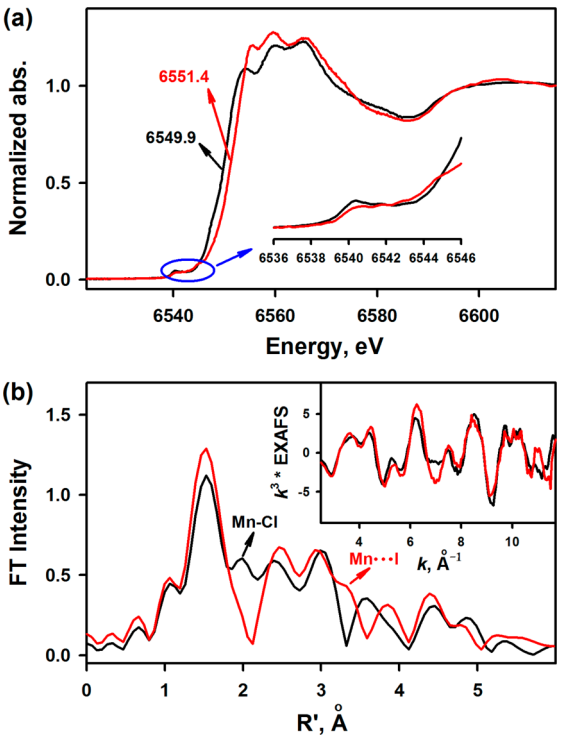

Figure 2. (a) Normalized Mn K-edge XAS data for [Mn^{III}(TDCPP)-Cl] (black line) and **1** (red line). Inset shows the expanded pre-edge region. (b) Non-phase-shift corrected Fourier transform data for [Mn^{III}(TDCPP)Cl] (black line) and **1** (red line). Inset shows the Mn K-edge EXAFS comparison.

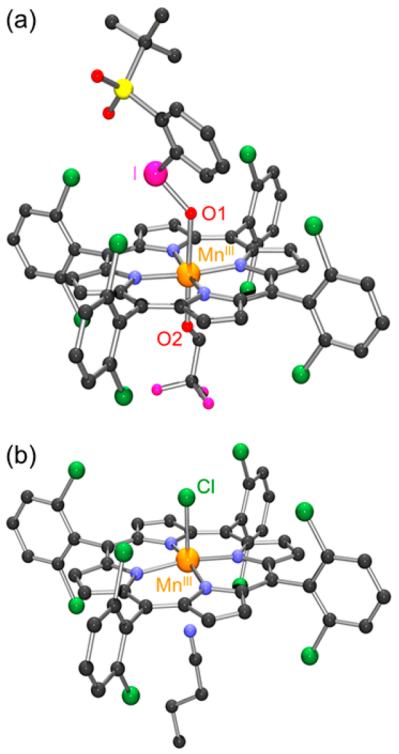

Figure 3. DFT-optimized structures of (a) **1**-$CF_3CH_2O^-$ and (b) [Mn^{III}(TDCPP)(Cl)](BuCN). Selected bond distances: Mn−O1 = 2.27 Å, Mn−O2 = 1.97 Å, and I−O1 = 1.89 Å for **1**-$CF_3CH_2O^-$ and Mn−Cl = 2.39 Å for [Mn^{III}(TDCPP)(Cl)](BuCN).

[Mn^{III}(TDCPP)Cl] are consistent with a first shell with 4 Mn−N at 2.00 Å and 1 Mn−Cl at 2.46 Å. The long Mn−Cl indicates weakening due to *trans*-axial solvent ligation. This is also consistent with the low pre-edge intensities observed in the XANES region.[19] In **1**, the first shell is fit with 5 Mn−N/O at 2.01 Å and a longer Mn−O at 2.28 Å. The best-fit also indicates the loss of Mn−Cl ligand present in the starting material. A long Mn···I interaction is observed at 3.89 Å.[20] For both of the species, robust single and multiple scattering contributions from the second and third shells of the porphyrin ligand were required to obtain a good fit (see Table S1 and Figures S4 and S5 in the SI). These data are in good agreement with the Mn K-pre-edge and rising-edge data and, together, are consistent with **1** being a Mn(III) complex coordinated by a ^{s}PhIO ligand.

To disambiguate *trans*-axial ligation and ^{s}PhIO ligand binding to the Mn center, density functional theory (DFT) calculations were performed on the starting [Mn^{III}(TDCPP)-Cl] and **1** with a range of possible *trans*-axial ligands, such as BuCN, H_2O, and TFE, and the results compared to the structures calculated without *trans*-axial ligands (see Figure 3 for the optimized structures). Time-dependent density functional theory (TD-DFT) calculations (not shown) were performed on the pre-edges to compare pre-edge intensity changes with *trans*-axial ligand coordination. The geometry-optimized structure and the pre-edge calculations are most consistent with very weak BuCN ligation to [Mn^{III}(TDCPP)-Cl] and with strong axial ligation of deprotonated $CF_3CH_2O^-$ to **1**. Theory reveals that **1** strongly binds to the $CF_3CH_2O^-$ ligand (Mn−O = 1.97 Å), which results in weaker binding of the ^{s}PhIO ligand (Mn−O = 2.27 Å). This is consistent with the EXAFS results, which show the appearance of an additional short Mn−N/O interaction at 2.01 Å and a longer Mn−O at 2.28 Å (see Table S1). In addition, EXAFS fitting of Mn(III)-mono-^{S}PhIO and Mn(III)-bis-^{s}PhIO species shows that the mono^{s}PhIO with solvent and the bis-^{s}PhIO give the best agreement with experiments, ruling out the other options (see Table S2 and Figures S5−S8 in the SI). Between these two possibilities, the mono^{s}PhIO with solvent gives the best result, and, combined with the other evidences, complex **1** is assigned to a Mn^{III}(TDCPP)-mono^{s}PhIO with solvent complex.

Conversion of Mn(III)-Iodosylarene Porphyrins to Mn-Oxo Porphyrins. Then, a question arises: How is the Mn(III)-iodosylarene porphyrin complex converted to high-valent Mn-oxo species? First, we investigated the porphyrin ligand effect on the stability of the Mn(III)-iodosylarene porphyrin complex. When [Mn^{III}(TPFPP)Cl],[14] which also bears an electron-deficient porphyrin ligand, reacted with ^{s}PhIO under the identical conditions, the formation of [Mn^{III}(^{s}PhIO)(TPFPP)]$^+$ was confirmed spectroscopically (see Figures S9−S11 in the SI). In contrast to the reactions of [Mn^{III}(TDCPP)Cl] and [Mn^{III}(TPFPP)Cl], when a manganese complex bearing an electron-rich porphyrin ligand (i.e., [Mn^{III}(TMP)Cl])[14] reacted with ^{s}PhIO, we observed the formation of [Mn^{IV}(O)(TMP)], not a Mn(III)-OIAr adduct, even at −80 °C (see Figure S12 in the SI),[21,22] resulting from a fast I−O bond cleavage of [Mn^{III}(^{s}PhIO)(TMP)]$^+$; it has been well-documented that the O−I (or O−O) bond cleavage of metal(III)−OIAr (or O−OH(R)) porphyrin complexes bearing electron-rich porphyrin ligands occurs at a fast rate.[5k] We also examined the temperature effect in the reaction of [Mn^{III}(TDCPP)Cl] and ^{s}PhIO. We have shown above that the reaction of [Mn^{III}(TDCPP)Cl] and ^{s}PhIO generated **1**, which

DOI: 10.1021/acs.inorgchem.8b01426
Inorg. Chem. XXXX, XXX, XXX−XXX

then decayed to [Mn^{IV}(O)(TDCPP)] (**2**) with a half-life of $t_{1/2} \approx 20$ min at −60 °C (see Figures S1a and S3b in the SI for spectroscopic characterization).[22,23] However, at a higher temperature (e.g., 0 °C), we observed the direct formation of **2**, because of the fast conversion from **1** to **2** at a high temperature (see Figures S1b and S13b in the SI (stopped flow)). Finally, we examined the effect of base (OH^-) on the formation of Mn(V)-oxo porphyrin species in the reaction of Mn(III) porphyrin complexes and ^{s}PhIO in the presence of a base.[23] When tetra-*n*-butylammonium hydroxide (TBAOH) was added to the solution of **1** at −60 °C, we observed the immediate formation of [Mn^{V}(O)(OH)(TDCPP)] (**3**) (see Figure S14a in the SI),[23] suggesting that the binding of OH^- *trans* to the Mn(III)-OIAr moiety cleaves the O−I bond to form **3** at a very fast rate. Therefore, we conclude that the stability of Mn(III)-iodosylarene complexes is significantly dependent on the electronic nature of porphyrin ligands, the reaction temperatures, and the binding of OH^- as an axial ligand.

Stoichiometric Oxidation of Olefins by Mn(III)-Iodosylarene Porphyrin Adduct. We then investigated the reactivity of **1** in olefin epoxidation reactions. Upon addition of cyclohexene to the solution of **1** at −60 °C, **1** was converted to the starting [Mn^{III}(TDCPP)]$^+$ complex with clean isosbestic points at 468 and 570 nm (see Figure 4). The

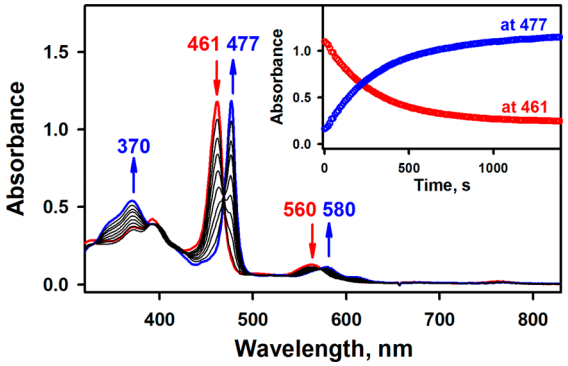

Figure 4. UV-vis spectral changes observed in the reaction of **1** (0.10 mM, red line) and cyclohexene (20 mM) in CH_2Cl_2/BuCN/TFE (v/v/v 5:5:1) at −60 °C. Inset shows the time traces monitored at 461 and 477 nm.

reaction rates for the decay of **1** and the regeneration of [Mn^{III}(TDCPP)]$^+$ were the same (Figure 4, inset), suggesting a direct transformation of **1** to the starting Mn(III) porphyrin complex in the oxidation of cyclohexene. By varying the concentration of cyclohexene, the second-order rate constant was determined to be $k_2 = 1.6 \times 10^{-1}$ M^{-1} s^{-1} at −60 °C (see Table 1, entry 1; also see Figure S15a in the SI). The second-order rate constant determined in the oxidation of deuterated cyclohexene, cyclohexene-d_{10}, by **1** was the same (see Table 1, entry 2; also see Figure S15a), giving a kinetic isotope effect (KIE) value of 1.0. In addition, product analysis of the reaction solutions revealed that cyclohexene oxide was the sole product formed in the oxidation of cyclohexene and cyclohexene-d_{10} by **1** (see Table 1, entries 1 and 2). These results demonstrate that the C=C double bond epoxidation pathway is preferred to the allylic C−H bond oxidation pathway in the oxidation of cyclohexene by **1**. Very recently, it has been shown that mononuclear nonheme metal(IV)-oxo and (13-TMC)Fe(III)-iodosylarene[14] complexes prefer the allylic C−H bond

Table 1. Second-Order Rate Constants and Products with Yields Obtained in the Stoichiometric Oxidation of Olefins by 1[a]

entry	substrate	k_2 (M^{-1} s^{-1})	product and yield[b] (%)
1	cyclohexene	1.6×10^{-1}	cyclohexene oxide (90)
2	cyclohexene-d_{10}	1.6×10^{-1}	cyclohexene oxide-d_{10} (91)
3	cyclooctene	1.9×10^{-1}	cyclooctene oxide (92)
4	styrene	1.2×10^{-1}	styrene oxide (92)
5	*cis*-stilbene	1.8×10^{-1}	*cis*-stilbene oxide (85)

[a]Reactions with **1** (0.10 mM) were performed in CH_2Cl_2/BuCN/TFE (v/v/v 5:5:1) at −60 °C. [b]Yields (shown in parentheses) were determined based on [**1**].

oxidation pathway to the C=C double bond epoxidation pathway in the oxidation of cyclohexene, giving high KIE values and allylic oxidation products, such as cyclohexenol and cyclohexenone.[12a,24,25]

Other olefins, such as cyclooctene, styrene, and *cis*-stilbene, were also oxidized by **1** at −60 °C, and their second-order rate constants and products are listed in Table 1 (also see Figures S15−S17 in the SI). It is worth noting that the formation of *trans*-stilbene oxide (and other possible byproducts such as benzaldehyde and phenylacetaldehyde)[26] was not detected in the oxidation of *cis*-stilbene by **1** (Table 1, entry 5), indicating that the olefin epoxidation reaction by **1** is highly stereoselective; *trans*-stilbene was also epoxidized to *trans*-stilbene oxide exclusively (data not shown). In addition, we obtained a ρ value of −0.6 from the Hammett plot of log k_2 against σ_p^+ in the epoxidation of *para*-X-substituted styrenes (see Figure S16 in the SI); the negative ρ value indicates electrophilic character of the Mn(III)-iodosylarene adduct species, as observed in the epoxidation of olefins by other metal-iodosylarene complexes[6,12a] and high-valent metal-oxo complexes.[27] In addition, the observation that the epoxidation rate is dependent on the electronic nature of substrates and the concentration of olefins indicates that the oxygen atom transfer from **1** to olefins is the rate-determining step (rds) (recall Scheme 1).

Catalytic Oxidation of Olefins by Mn(III) Porphyrins and ^{s}PhIO. We then performed catalytic reactions under various conditions to understand the nature of oxidizing species involved in the catalytic oxidation of olefins by Mn(III) porphyrins and ^{s}PhIO. The addition of ^{s}PhIO (10 mM; 50 equiv to the catalyst) to a reaction solution containing [Mn^{III}(TDCPP)Cl] (0.20 mM) and cyclohexene (200 mM) at −60 °C afforded the immediate formation of **1**. The UV-vis spectrum of the reaction solution remained the same for ∼3 h, followed by the decay of **1** and the concurrent regeneration of [Mn^{III}(TDCPP)Cl] after the complete consumption of ^{s}PhIO (Figure 5, open circles); this observation indicates that **1** is in the steady state during the catalytic reaction. In addition, the duration of the steady state was dependent on the amount of ^{s}PhIO employed. When 4 mM of ^{s}PhIO (20 equiv to the catalyst) was employed under the same conditions, the lifetime of **1** in the catalytic reaction was shortened to ∼3000 s (Figure 5, closed circles). Product analysis of the reaction solution revealed that cyclohexene oxide was the only product yielded in the catalytic reactions, affording a moderate yield of 45%, compared to other manganese-complex-catalyzed epoxidation reactions (see Table 2, entry 1).[5b,e] These results demonstrate unambiguously that **1** is the active oxidant involved as an active oxidant in the catalytic epoxidation reaction.

DOI: 10.1021/acs.inorgchem.8b01426
Inorg. Chem. XXXX, XXX, XXX−XXX

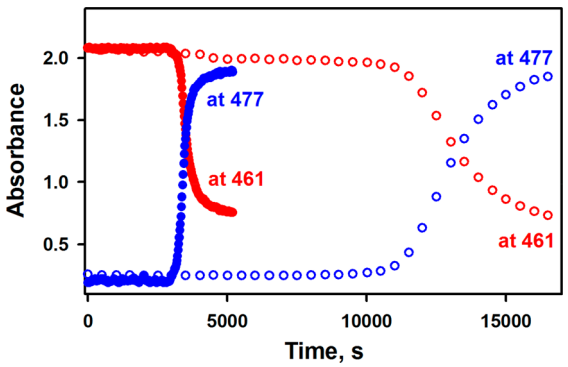

Figure 5. Time profiles monitored at 461 nm due to **1** (red open or closed circles) and 477 nm due to [Mn^{III}(TDCPP)Cl] (blue open or closed circles) observed in the catalytic oxidation of cyclohexene (200 mM) by [Mn^{III}(TDCPP)Cl] (0.20 mM) with ^{s}PhIO [10 mM (open circles) and 4.0 mM (closed circles)] in CH_2Cl_2/BuCN/TFE (v/v/v 5:5:1) at −60 °C.

Table 2. Products with Yields Obtained in the Catalytic Oxidation of Cyclohexene by Mn(III) Porphyrin Complexes and ^{s}PhIO[a]

entry	catalyst	temperature (°C)	product and yield[b] (%)
1	[Mn^{III}(TDCPP)Cl]	−60	cyclohexene oxide (45)
2	[Mn^{III}(TDCPP)Cl]	0	cyclohexene oxide (30) cyclohex-2-enol (17) cyclohex-2-enone (3)
3	[Mn^{III}(TMP)Cl]	−60	cyclohexene oxide (27) cyclohex-2-enol (30) cyclohex-2-enone (4)
4	[Mn^{III}(TMP)Cl]	0	cyclohexene oxide (27) cyclohex-2-enol (26) cyclohex-2-enone (6)

[a][catalyst] = 0.20 mM, [^{s}PhIO] = 10 mM, and [cyclohexene] = 200 mM were used in the catalytic oxidation in CH_2Cl_2/BuCN/TFE (v/v/v 5:5:1). [b]Yields (shown in parentheses) were determined based on [^{s}PhIO].

When the catalytic oxidation of cyclohexene by [Mn^{III}(TDCPP)Cl] and ^{s}PhIO was performed at 0 °C, the formation of **1** was not observed under the conditions (see Figure S18 in the SI). Product analysis revealed the formation of cyclohexene oxide (30%), along with allylic oxidation products, such as cyclohex-2-enol (17%) and cyclohex-2-enone (6%) (Table 2, entry 2). The latter result suggests that the allylic C−H bond oxidation pathway competes with the C=C double bond epoxidation pathway at a high temperature (e.g., 0 °C). Similarly, when [Mn^{III}(TMP)Cl] was employed as a catalyst instead of [Mn^{III}(TDCPP)Cl], allylic oxidation products along with cyclohexene oxide were obtained, irrespective of reaction temperatures (e.g., −60 and 0 °C) (Table 2, entries 3 and 4). As we have shown in the formation of [Mn^{IV}(O)(TMP)] in the reaction of [Mn^{III}(TMP)Cl] and ^{s}PhIO at −60 °C under the stoichiometric conditions (vide supra), we observed the [Mn^{IV}(O)(TMP)] species in the catalytic reactions for a short time at −60 °C (see Figure S19 in the SI). Therefore, in sharp contrast to the catalytic reaction of [Mn^{III}(TDCPP)Cl] at −60 °C, the results of the reactions of [Mn^{III}(TDCPP)Cl] at 0 °C and [Mn^{III}(TMP)Cl] at −60 and 0 °C suggest that the active oxidant(s) involved in these reactions may not be the Mn(III)-iodosylarene adduct but a high-valent Mn(IV or V) species that is generated via a fast I−O bond cleavage; the conversion of Mn(III)-iodosylarene to Mn(IV)-oxo species at a fast rate was shown in the reactions of using a Mn complex with an electron-rich porphyrin ligand and at a higher temperature (vide supra). Based on the results presented above, we conclude that multiple oxidants are involved in the catalytic oxidation of cyclohexene by iodosylarenes and the nature of the active oxidants varies, depending on the reaction conditions.

CONCLUSION

In summary, we have reported, for the first time, the synthesis and characterization of a mononuclear Mn(III)-iodosylarene adduct bearing an electron-deficient porphyrin ligand. By utilizing the spectroscopically well-characterized Mn(III)-iodosylarene species in reactivity studies, we were able to conclude that this Mn(III)-iodosylarene porphyrin complex is capable of conducting the epoxidation of olefins with high chemoselectivities and stereoselectivities. We have also demonstrated that this Mn(III)-iodosylarene porphyrin complex is involved as an active oxidant in the catalytic oxidation of olefins at a low temperature. In the catalytic reaction at a high temperature, however, the Mn(III)-iodosylarene porphyrin complex is converted to high-valent Mn-oxo porphyrin species that affects the cyclohexene oxidation. In addition, in the case of Mn(III) catalyst bearing an electron-rich porphyrin ligand, Mn-oxo species, which is formed via O−I bond cleavage at a fast rate, becomes an active oxidant irrespective of reaction temperatures. Thus, the latter results provide clues to resolve the long-standing controversy on the single oxidant versus multiple oxidants debate in heme systems.

EXPERIMENTAL SECTION

Materials. Organic compounds were purchased from Aldrich and TCI with the maximum purity available and used as received, unless otherwise indicated. Solvents were dried according to the literature procedures and redistilled under an argon atmosphere before use.[28] All reactions were performed under argon atmosphere using dried solvent and standard Schlenk techniques, unless otherwise noted. 1-(*tert*-butylsulfonyl)-2-iodosylbenzene (^{s}PhIO) was synthesized by a literature method.[13] Mn(III)-porphyrin complexes were purchased from Frontier Scientific, Inc. $H_2{}^{18}O$ (95% ^{18}O-enriched) was purchased from ICON Services, Inc. (Summit, NJ).

Instrumentation. UV-vis spectra were recorded on a Hewlett−Packard Agilent 8453 UV-vis spectrophotometer equipped with an UNISOKU cryostat system (Model USP-203, UNISOKU, Japan) or on a Hi-Tech Scientific (UK) Model SF-61 DX2 cryogenic stopped-flow spectrometer that was equipped with a Xe arc lamp and a KinetaScan diode array rapid scanning unit. Coldspray ionization mass spectroscopy (CSI-MS) data were collected on a Model JMS-T100CS (JEOL) mass spectrometer that was equipped with a CSI source [conditions: needle voltage = 2.2 kV, orifice 1 current = 50−500 nA, orifice 1 voltage = 0−20 V, ringlens voltage = 10 V, ion source temperature = 5 °C, spray temperature = −40 °C]. Raman spectra were obtained using a liquid-nitrogen-cooled CCD detector (CCD-1024 × 256-OPEN-1LS, HORIBA Jobin Yvon) attached to a 1-m single polychromator (Model MC-100DG, Ritsu Oyo, Kogaku, Japan) with a 1200 grooves/mm holographic grating. Excitation wavelength of 441.6 nm was provided by He−Cd laser (Kimmon Koha, Model IK4101R-F) with 20 mW power at the sample point. Raman shifts were calibrated with indene, and the accuracy of the peak positions of the Raman bands was ±1 cm^{-1}. X-band electron

DOI: 10.1021/acs.inorgchem.8b01426
Inorg. Chem. XXXX, XXX, XXX−XXX

paramagnetic resonance (EPR) spectra were recorded at 5 K using an X-band Bruker EMX-plus spectrometer equipped with a dual-mode cavity (Model ER 4116DM) [experimental parameters: microwave frequency = 9.647 GHz, microwave power = 1.0 mW, modulation amplitude = 10 G, gain = 1×10^4, modulation frequency = 100 kHz, time constant = 40.96 ms, conversion time = 85.00 ms]. Low temperatures for EPR were achieved and controlled with an Oxford Instruments Model ESR900 liquid He quartz cryostat with an Oxford Instruments Model ITC503 temperature and gas flow controller. Product analysis was performed on an Agilent Model GC-6890 chromatograph, using a CP-ChirasilDex CB column (25 m × 0.32 mm i.d.; 0.25 μm film thickness) or high-performance liquid chromatography (HPLC) (DIOMEX Pump Series P580) that was equipped with a variable-wavelength UV-200 detector and Diacel OD-H column (4.6 mm × 25 cm), the mobile phase was a mixture of methanol/water (1:1 or 3:1) at a flow rate of 1.0 mL/min. The product was identified by comparison to the GC or HPLC retention time.

Generation of Mn(III)-Iodosylarene Adduct Complexes. The Mn(III)-iodosylarene adduct intermediate, $[Mn^{III}(^{s}PhIO)(TDCPP)]^+$ (**1**) was generated by adding ^{s}PhIO (0.50 mM) into a 1 mm UV-vis cuvette containing a CH_2Cl_2/BuCN/TFE (v/v/v 5:5:1) mixed solution of $[Mn^{III}(TDCPP)Cl]$ (0.10 mM) at −60 °C. Formation of **1** was confirmed by monitoring UV-vis spectral changes for the formation of absorption bands at 461 and 560 nm due to **1** and the decay of absorption bands at 477 and 580 nm due to $[Mn^{III}(TDCPP)Cl]$. $[Mn^{III}(^{s}PhIO)(TPFPP)]^+$ was also generated using $[Mn^{III}(TPFPP)Cl]$ via the same procedure for **1**.

Generation of Mn^{IV}−Oxo Species. $[Mn^{IV}(O)(TDCPP)]$ (**2**) was generated by adding ^{s}PhIO (0.50 mM) into a 1 mm UV-vis cuvette containing a CH_2Cl_2/BuCN/TFE (v/v/v 5:5:1) mixed solution of $[Mn^{III}(TDCPP)Cl]$ (0.10 mM) at 0 °C. Formation of **2** was confirmed by monitoring UV-vis spectral changes for the formation of absorption bands at 422 and 520 nm due to **2** and the decay of absorption bands at 477 and 580 nm due to $[Mn^{III}(TDCPP)Cl]$. $[Mn^{IV}(O)(TPFPP)]$ and $[Mn^{IV}(O)(TMP)]$ were also prepared using $[Mn^{III}(TPFPP)Cl]$ and $[Mn^{III}(TMP)Cl]$, respectively, by the same procedure for **2**.

Generation of $Mn^{V}(O)(OH)$ Species. $[Mn^{V}(O)(OH)(TDCPP)]$ (**3**) was prepared by adding ^{s}PhIO (0.50 mM) into a 1 mm UV-vis cuvette containing a CH_2Cl_2/BuCN/TFE (v/v/v 5:5:1) mixed solution of $[Mn^{III}(TDCPP)Cl]$ (0.10 mM) in the presence of tetra-*n*-butylammonium hydroxide (TBAOH; 5.0 mM) at 25 °C. Formation of **3** was confirmed by monitoring UV-vis spectral changes for the formation of absorption bands at 441 and 557 nm due to **3** and the decay of absorption bands at 477 and 580 nm due to $[Mn^{III}(TDCPP)Cl]$. **3** could also be obtained by adding TBAOH (5.0 mM) to a solution of **1** (0.10 mM) at −60 °C, which was prepared from $[Mn^{III}(TDCPP)Cl]$ with ^{s}PhIO.

Mn K-edge XANES and EXAFS Measurements. The Mn K-edge X-ray absorption spectra of $[Mn^{III}(TDCPP)Cl]$ and **1** were measured at the Stanford Synchrotron Radiation Lightsource (SSRL) on the BL7−3 wiggler under standard ring conditions of 3 GeV and ∼500 mA. A Si(220) double crystal monochromator was used for energy selection. The monochromator was detuned by 40% to reject components of harmonic components from data contamination. During data collection, the samples were maintained at a constant temperature of ∼10 K using a CryoIndustries closed cycle cryocooler. A 30-element Ge fluorescence detector from Canberra Industries was employed for fluorescence data measurement to k = 12 Å^{-1}. Background signal was suppressed by using soller slits equipped with a Cr filter. Solution samples for $[Mn^{III}(TDCPP)Cl]$ and intermediate **1** were transferred into 2 mm delrin XAS cells with 70 m Kapton tape windows under synthesis conditions and were immediately frozen after preparation and stored under liquid N_2 conditions. Internal energy calibration was accomplished by simultaneous measurement of the absorption of a Mn foil placed between two ionization chambers situated after the sample. The first inflection point of the foil spectrum was set at 6539.0 eV. Data presented here are 8-scan average spectra for $[Mn^{III}(TDCPP)Cl]$ and 9-scan average spectrum for **1**. To avoid potential photodamage, at most, two scans were obtained on a fresh sample. A small shift in the rising edge position indicated photoreduction (judging by comparison of scan 1 and scan 2) and the edge data presented here are the average of the first scans from each fresh sample. The first scan average EXAFS data were also compared with the average from the complete set, without any noticeable difference; hence, a complete dataset was used for EXAFS analysis for both $[Mn^{III}(TDCPP)Cl]$ and **1**. Data were processed by fitting a second-order polynomial to the pre-edge region and then subtracting this from the entire spectrum as background. A three-region spline of orders 2, 3, and 3 was used to model the smoothly decaying post-edge region. The data were normalized by subtracting the cubic spline and assigning the edge jump to 1.0 at 6555 eV using the Pyspline[29] program. Data were then renormalized in Kaleidagraph for comparison and quantitation purposes. Theoretical EXAFS signals $\chi(k)$ were calculated by using FEFF[30−32] (Macintosh version), using geometry optimized preliminary structures obtained from density functional theory (DFT) calculations. The input structure was improved based on preliminary EXAFS fit parameters to generate more-accurate theoretical EXAFS signals. Data fitting was performed in EXAFSPAK.[33] The structural parameters varied during the fitting process were the bond distance (R) and the bond variance σ^2, which is related to the Debye−Waller factor resulting from thermal motion, and static disorder of the absorbing and scattering atoms. The nonstructural parameter E_0 (the energy at which k = 0) was also allowed to vary but was restricted to a common value for every component in a given fit. Coordination numbers was systematically varied in the course of the fit but were fixed within a given fit.

Theoretical Calculations. Gradient-corrected, (GGA) spin-unrestricted DFT calculations were performed using ORCA 3.03.[34] The BP86[35,36] local functional and the following basis sets were employed for the calculations: Ahlrich's all-electron triple-ζ basis set TZVPPP[37−39] with three polarization functions on Mn, TZVP on all other atoms. Tight convergence criteria were imposed on all calculations. Starting guess geometries were obtained from the respective crystal structures and modified appropriately where needed. Time-dependent density functional theory (TD-DFT) calculations were performed with the electronic structure program ORCA to calculate the energies and intensities of the Mn K pre-edges. The tight convergence criterion was imposed on all calculations. The same functional and basis sets were used as the geometry optimizations. The calculated energies and intensities were Gaussian-broadened with half-widths of 1.3 eV to account for core−hole lifetime and instrument resolution. The calculated pre-edge energy positions were linearly scaled to match the experimental spectra. The TD-DFT results were compared with experimental data to judge the efficacy of the DFT calculation.

Kinetic Studies for the Epoxidation of Olefins by 1. Olefins, such as cyclohexene, cyclooctene, styrene, styrene derivatives, and *cis*-stilbene, were added into a 1-mm UV-vis cuvette containing a CH_2Cl_2/BuCN/TFE (v/v/v 5:5:1) mixed solution of **1** (0.10 mM) at −60 °C. The kinetic studies were followed by monitoring the change of the absorption band at 461 nm, because of the decay of **1**. The kinetic experiments were run at least in triplicate, and the data reported here represented the average of these reactions. Rate constants were determined under pseudo-first-order conditions (i.e., [substrate]/[**1**] > 10) by fitting the absorbance changes at 461 nm due to the decay of **1**. The kinetic isotope effect (KIE) was determined by comparing the decay rates of **1** observed in the oxidation of cyclohexene and cyclohexene-d_{10} by **1**.

Catalytic Oxidation of Olefins by Mn(III)-Porphyrin Complexes with ^{s}PhIO. ^{s}PhIO (10 mM) was added into a CH_2Cl_2/BuCN/TFE (v/v/v 5:5:1) solution containing Mn(III)-porphyrin complexes (0.20 mM), such as $[Mn^{III}(TDCPP)Cl]$ and $[Mn^{III}(TMP)Cl]$, and cyclohexene (200 mM) at −60 and 0 °C.

Product Analysis. For stoichiometric epoxidation, when the reaction was complete as indicated by the spectral changes, internal standard (decane) was added to the solution. For catalytic oxidations, when the reactions were carried out at −60 and 0 °C, the internal

DOI: 10.1021/acs.inorgchem.8b01426
Inorg. Chem. XXXX, XXX, XXX−XXX

standard (decane) was added to the reaction solution after 4 and 1 h, respectively. The reaction solution was filtered through a basic alumina plug and analyzed by GC for the reactions with cyclohexene, styrene, and styrene derivatives and HPLC for the reaction with *cis*-stilbene. Products were identified by comparing with authentic samples, and product yields were determined by comparing peak areas with that of decane, which was used as an internal standard.

■ ASSOCIATED CONTENT

Supporting Information

The Supporting Information is available free of charge on the ACS Publications website at DOI: 10.1021/acs.inorgchem.8b01426.

EXAFS data (Table S1) and spectroscopic characterization and kinetic data (Figures S1−S19) (PDF)

■ AUTHOR INFORMATION

Corresponding Authors

*E-mail: ritis@slac.stanford.edu (R. Sarangi).
*E-mail: fukuzumi@chem.eng.osaka-u.ac.jp (S. Fukuzumi).
*E-mail: wwnam@ewha.ac.kr (W. Nam).

ORCID

Yong-Min Lee: 0000-0002-5553-1453
Takehiro Ohta: 0000-0003-4140-5293
Won-Suk Kim: 0000-0001-9180-4570
Ritimukta Sarangi: 0000-0002-2764-2279
Shunichi Fukuzumi: 0000-0002-3559-4107
Wonwoo Nam: 0000-0001-8592-4867

Notes

The authors declare no competing financial interest.

■ ACKNOWLEDGMENTS

This work was supported by the NRF of Korea through CRI (No. NRF-2012R1A3A2048842 to W.N.), GRL (No. NRF-2010-00353 to W.N.), and Basic Science Research Program (No. 2017R1D1A1B03029982 to Y.-M.L. and No. 2017R1D1A1B03032615 to S.F.). The SSRL SMB resource is supported by the NIH National Institute of General Medical Sciences (NIGMS) through a Biomedical Technology Research Resource P41 grant (No. P41GM103393) and by the DOE Office of Biological and Environmental Research.

■ REFERENCES

(1) (a) Meunier, B. *Biomimetic Oxidations Catalyzed by Transition Metal Complexes*; Imperial College Press: London, 2000. (b) Que, L., Jr.; Tolman, W. B. Biologically inspired oxidation catalysis. *Nature* **2008**, *455*, 333−340.

(2) (a) Huang, X.; Groves, J. T. Oxygen Activation and Radical Transformations in Heme Proteins and Metalloporphyrins. *Chem. Rev.* **2018**, *118*, 2491−2553. (b) Wang, V. C. C.; Maji, S.; Chen, P. P. Y.; Lee, H. K.; Yu, S. S. F.; Chan, S. I. Alkane Oxidation: Methane Monooxygenases, Related Enzymes, and Their Biomimetics. *Chem. Rev.* **2017**, *117*, 8574−8621. (c) Schwizer, F.; Okamoto, Y.; Heinisch, T.; Gu, Y.; Pellizzoni, M. M.; Lebrun, V.; Reuter, R.; Köhler, V.; Lewis, J. C.; Ward, T. R. Artificial Metalloenzymes: Reaction Scope and Optimization Strategies. *Chem. Rev.* **2018**, *118*, 142−231.

(3) (a) Baglia, R. A.; Zaragoza, J. P. T.; Goldberg, D. P. Biomimetic Reactivity of Oxygen-Derived Manganese and Iron Porphyrinoid Complexes. *Chem. Rev.* **2017**, *117*, 13320−13352. (b) Engelmann, X.; Monte-Pérez, I.; Ray, K. Oxidation Reactions with Bioinspired Mononuclear Non-Heme Metal−Oxo Complexes. *Angew. Chem., Int. Ed.* **2016**, *55*, 7632−7649. (c) Nam, W. Synthetic Mononuclear Nonheme Iron−Oxygen Intermediates. *Acc. Chem. Res.* **2015**, *48*, 2415−2423. (d) Oloo, W. N.; Que, L., Jr. Bioinspired Nonheme Iron Catalysts for C−H and C = C Bond Oxidation: Insights into the Nature of the Metal-Based Oxidants. *Acc. Chem. Res.* **2015**, *48*, 2612−2621. (e) Chen, Z.; Yin, G. The Reactivity of the Active Metal Oxo and Hydroxo Intermediates and Their Implications in Oxidations. *Chem. Soc. Rev.* **2015**, *44*, 1083−1100. (f) Ray, K.; Pfaff, F. F.; Wang, B.; Nam, W. Status of Reactive Non-Heme Metal−Oxygen Intermediates in Chemical and Enzymatic Reactions. *J. Am. Chem. Soc.* **2014**, *136*, 13942−13958. (g) Yin, G. Understanding the Oxidative Relationships of the Metal Oxo, Hydroxo, and Hydroperoxide Intermediates with Manganese(IV) Complexes Having Bridged Cyclams: Correlation of the Physicochemical Properties with Reactivity. *Acc. Chem. Res.* **2013**, *46*, 483−492. (h) Nam, W. High-Valent Iron(IV)−Oxo Complexes of Heme and Non-Heme Ligands in Oxygenation Reactions. *Acc. Chem. Res.* **2007**, *40*, 522−531.

(4) (a) Song, W.; Ryu, Y.; Song, R.; Nam, W. Oxoiron(IV) Porphyrin π-Cation Radical Complexes with a Chameleon Behavior in Cytochrome P450 Model Reactions. *J. Biol. Inorg. Chem.* **2005**, *10*, 294−304. (b) Nam, W.; Ryu, Y.; Song, W. Oxidizing intermediates in cytochrome P450 model reactions. *J. Biol. Inorg. Chem.* **2004**, *9*, 654−660.

(5) (a) Kang, Y.; Li, X.-X.; Cho, K.-B.; Sun, W.; Xia, C.; Nam, W.; Wang, Y. Mutable Properties of Nonheme Iron(III)−Iodosylarene Complexes Result in the Elusive Multiple-Oxidant Mechanism. *J. Am. Chem. Soc.* **2017**, *139*, 7444−7447. (b) Leeladee, P.; Goldberg, D. P. Epoxidations Catalyzed by Manganese(V) Oxo and Imido Complexes: Role of the Oxidant-Mn-Oxo (Imido) Intermediate. *Inorg. Chem.* **2010**, *49*, 3083−3085. (c) Yin, G.; Buchalova, M.; Danby, A. M.; Perkins, C. M.; Kitko, D.; Carter, J. D.; Scheper, W. M.; Busch, D. H. Olefin Oxygenation by the Hydroperoxide Adduct of a Nonheme Manganese(IV) Complex: Epoxidations by a Metallo-Peracid Produces Gentle Selective Oxidations. *J. Am. Chem. Soc.* **2005**, *127*, 17170−17171. (d) Wang, S. H.; Mandimutsira, B. S.; Todd, R.; Ramdhanie, B.; Fox, J. P.; Goldberg, D. P. Catalytic Sulfoxidation and Epoxidation with a Mn(III) Triazacorrole: Evidence for A "Third Oxidant" in High-Valent Porphyrinoid Oxidations. *J. Am. Chem. Soc.* **2004**, *126*, 18−19. (e) Collman, J. P.; Zeng, L.; Brauman, J. I. Donor Ligand Effect on the Nature of the Oxygenating Species in Mn^{III}(salen)-Catalyzed Epoxidation of Olefins: Experimental Evidence for Multiple Active Oxidants. *Inorg. Chem.* **2004**, *43*, 2672−2679. (f) Bryliakov, K. P.; Talsi, E. P. Evidence for the Formation of an Iodosylbenzene(salen)iron Active Intermediate in a (Salen)iron-(III)-Catalyzed Asymmetric Sulfide Oxidation. *Angew. Chem., Int. Ed.* **2004**, *43*, 5228−5230. (g) Newcomb, M.; Hollenberg, P. F.; Coon, M. J. Multiple Mechanisms and Multiple Oxidants in P450-Catalyzed Hydroxylations. *Arch. Biochem. Biophys.* **2003**, *409*, 72−79. (h) Collman, J. P.; Zeng, L.; Decreau, R. A. Multiple Active Oxidants in Competitive Epoxidations Catalyzed by Porphyrins and Corroles. *Chem. Commun.* **2003**, 2974−2975. (i) Collman, J. P.; Chien, A. S.; Eberspacher, T. A.; Brauman, J. I. Multiple Active Oxidants in Cytochrome P-450 Model Oxidations. *J. Am. Chem. Soc.* **2000**, *122*, 11098−11100. (j) Nam, W.; Lim, M. H.; Lee, H. J.; Kim, C. Evidence for the Participation of Two Distinct Reactive Intermediates in Iron(III) Porphyrin Complex-Catalyzed Epoxidation Reactions. *J. Am. Chem. Soc.* **2000**, *122*, 6641−6647. (k) Machii, K.; Watanabe, Y.; Morishima, I. Acylperoxo-Iron(III) Porphyrin Complexes: A New Entry of Potent Oxidants for the Alkene Epoxidation. *J. Am. Chem. Soc.* **1995**, *117*, 6691−6697.

(6) (a) Collman, J. P.; Zeng, L.; Wang, H. J. H.; Lei, A.; Brauman, J. I. Kinetics of (Porphyrin)manganese(III)-Catalyzed Olefin Epoxidation with a Soluble Iodosylbenzene Derivative. *Eur. J. Org. Chem.* **2006**, *2006*, 2707−2714. (b) Araki, I.; Fukui, K.; Fujii, H. Preparation, Characterization and Reactivity of a Bis-hypochlorite Adduct of a Chiral Manganese(IV) Salen Complex. *Inorg. Chem.* **2018**, *57*, 1685−1688. (c) Cong, Z.; Yanagisawa, S.; Kurahashi, T.; Ogura, T.; Nakashima, S.; Fujii, H. Synthesis, Characterization, and Reactivity of Hypochloritoiron(III) Porphyrin Complexes. *J. Am. Chem. Soc.* **2012**, *134*, 20617−20620.

DOI: 10.1021/acs.inorgchem.8b01426
Inorg. Chem. XXXX, XXX, XXX−XXX

(7) (a) Yoshimura, A.; Zhdankin, V. V. Advances in Synthetic Applications of Hypervalent Iodine Compounds. *Chem. Rev.* **2016**, *116*, 3328−3435. (b) Zhdankin, V. V.; Stang, P. J. Chemistry of Polyvalent Iodine. *Chem. Rev.* **2008**, *108*, 5299−5358. (c) Stang, P. J.; Zhdankin, V. V. Organic Polyvalent Iodine Compounds. *Chem. Rev.* **1996**, *96*, 1123−1178.

(8) (a) Wang, B.; Lee, Y.-M.; Tcho, W.-Y.; Tussupbayev, S.; Kim, S.-T.; Kim, Y.; Seo, M. S.; Cho, K.-B.; Dede, Y.; Keegan, B. C.; Ogura, T.; Kim, S. H.; Ohta, T.; Baik, M.-H.; Ray, K.; Shearer, J.; Nam, W. Synthesis and Reactivity of a Mononuclear Non-haem Cobalt(IV)-Oxo Complex. *Nat. Commun.* **2017**, *8*, 14839. (b) Nam, W.; Choi, S. K.; Lim, M. H.; Rohde, J.-U.; Kim, I.; Kim, J.; Kim, C.; Que, L., Jr. Reversible Formation of Iodosylbenzene-Iron Porphyrin Intermediates in the Reaction of Oxoiron(IV) Porphyrin π-Cation Radicals and Iodobenzene. *Angew. Chem., Int. Ed.* **2003**, *42*, 109−111. (c) Gross, Z.; Golubkov, G.; Simkhovich, L. Epoxidation Catalysis by a Manganese Corrole and Isolation of an Oxomanganese(V) Corrole. *Angew. Chem., Int. Ed.* **2000**, *39*, 4045−4047.

(9) (a) Wang, C.; Kurahashi, T.; Inomata, K.; Hada, M.; Fujii, H. Oxygen-Atom Transfer from Iodosylarene Adducts of a Manganese-(IV) Salen Complex: Effect of Arenes and Anions on I(III) of the Coordinated Iodosylarene. *Inorg. Chem.* **2013**, *52*, 9557−9566. (b) Wang, C.; Kurahashi, T.; Fujii, H. Structure and Reactivity of an Iodosylarene Adduct of a Manganese(IV)−Salen Complex. *Angew. Chem., Int. Ed.* **2012**, *51*, 7809−7811.

(10) Smegal, J. A.; Hill, C. L. Synthesis, Characterization, and Reaction Chemistry of a Bis(iodosylbenzene)-Metalloporphyrin Complex, $[PhI(OAC)O]_2Mn^{IV}TPP$. A Complex Possessing a Five-Electron Oxidation Capability. *J. Am. Chem. Soc.* **1983**, *105*, 2920−2922.

(11) (a) Lennartson, A.; McKenzie, C. J. An Iron(III) Iodosylbenzene Complex: A Masked Non-Heme $Fe^{V}O$. *Angew. Chem., Int. Ed.* **2012**, *51*, 6767−6770. (b) de Sousa, D. P.; Wegeberg, C.; Vad, M. S.; Mørup, S.; Frandsen, C.; Donald, W. A.; McKenzie, C. J. Halogen-Bonding-Assisted Iodosylbenzene Activation by a Homogenous Iron Catalyst. *Chem.—Eur. J.* **2016**, *22*, 3810−3820. (c) Au-Yeung, K.-C.; So, Y.-M.; Wang, G.-C.; Sung, H. H. Y.; Williams, I. D.; Leung, W.-H. Iodosylbenzene and Iodylbenzene Adducts of Cerium(IV) Complexes Bearing Chelating Oxygen Ligands. *Dalton Trans.* **2016**, *45*, 5434−5438. (d) Turlington, C. R.; Morris, J.; White, P. S.; Brennessel, W. W.; Jones, W. D.; Brookhart, M.; Templeton, J. L. Exploring Oxidation of Half-Sandwich Rhodium Complexes: Oxygen Atom Insertion into the Rhodium-Carbon Bond of κ^2-Coordinated 2-Phenylpyridine. *Organometallics* **2014**, *33*, 4442−4448. (e) de Ruiter, G.; Carsch, K. M.; Gul, S.; Chatterjee, R.; Thompson, N. B.; Takase, M. K.; Yano, J.; Agapie, T. Accelerated Oxygen Atom Transfer and C−H Bond Oxygenation by Remote Redox Changes in Fe_3Mn-Iodosobenzene Adducts. *Angew. Chem., Int. Ed.* **2017**, *56*, 4772−4776.

(12) (a) Wang, B.; Lee, Y.-M.; Seo, M. S.; Nam, W. Mononuclear Nonheme Iron(III)-Iodosylarene and High-Valent Iron-Oxo Complexes in Olefin Epoxidation Reactions. *Angew. Chem., Int. Ed.* **2015**, *54*, 11740−11744. (b) Hong, S.; Wang, B.; Seo, M. S.; Lee, Y.-M.; Kim, M. J.; Kim, H. R.; Ogura, T.; Garcia-Serres, R.; Clémancey, M.; Latour, J.-M.; Nam, W. Highly Reactive Nonheme Iron(III) Iodosylarene Complexes in Alkane Hydroxylation and Sulfoxidation Reactions. *Angew. Chem., Int. Ed.* **2014**, *53*, 6388−6392.

(13) Guo, M.; Dong, H.; Li, J.; Cheng, B.; Huang, Y.-q.; Feng, Y.-q.; Lei, A. Spectroscopic Observation of Iodosylarene Metalloporphyrin Adducts and Manganese(V)-Oxo Porphyrin Species in a Cytochrome P450 Analogue. *Nat. Commun.* **2012**, *3*, 1190.

(14) Abbreviations used: TDCPP, *meso*-tetrakis(2,6-dichlorophenyl) porphinato dianion; TPFPP, *meso*-tetrakis(pentafluorophenyl)porphinato dianion; TMP, *meso*-tetramesitylporphinato dianion; 13-TMC, 1,4,7,10-tetramethyl-1,4,7,10-tetraazacyclotridecane.

(15) Identical UV-vis spectrum and reactivity performance of **1** could be obtained in neat CH_2Cl_2 at −60 °C. However, the solvent system was optimized to be CH_2Cl_2/BuCN/TFE (v/v/v 5:5:1), because of the characterization, such as CSI-MS and rRaman spectroscopy.

(16) (a) Guo, M.; Lee, Y.-M.; Gupta, R.; Seo, M. S.; Ohta, T.; Wang, H.-H.; Liu, H.-Y.; Dhuri, S. N.; Sarangi, R.; Fukuzumi, S.; Nam, W. Dioxygen Activation and O−O Bond Formation Reactions by Manganese Corroles. *J. Am. Chem. Soc.* **2017**, *139*, 15858−15867. (b) Sarangi, R. X-ray Absorption Near-Edge Spectroscopy in Bioinorganic Chemistry: Application to $M-O_2$ Systems. *Coord. Chem. Rev.* **2013**, *257*, 459−472.

(17) Ganguly, S.; Renz, D.; Giles, L. J.; Gagnon, K. J.; McCormick, L. J.; Conradie, J.; Sarangi, R.; Ghosh, A. Cobalt- and Rhodium-Corrole-Triphenylphosphine Complexes Revisited: The Question of a Noninnocent Corrole. *Inorg. Chem.* **2017**, *56*, 14788−14800.

(18) Note that a shift in rising edge to higher energies may also indicate an increase in oxidation state; however, this primarily applies to like-ligand systems.

(19) A weak *trans*-axial solvent ligand is typically not observed in solution EXAFS measurements of transition metal-porphyrin complexes.

(20) The error in the Mn−I distance is large (0.05−0.08 Å) because of two factors: (i) the Mn and I do not share a bond and the interatomic distance is long, and (ii) its scattering contribution overlaps with the porphyrin robust multiple scattering

(21) Groves, J. T.; Stern, M. K. Synthesis, Characterization, and Reactivity of Oxomanganese(IV) Porphyrin Complexes. *J. Am. Chem. Soc.* **1988**, *110*, 8628−8638.

(22) Very recently, Yokota and Fujii reported mechanistic studies on the formation of Fe(IV)(O)(Porp) and $[Fe(IV)(O)(Porp^{\bullet+})]^+$ species from its Fe(III)(OCl)(Porp) precursor; see: Yokota, S.; Fujii, H. Critical Factors in Determining the Heterolytic versus Homolytic Bond Cleavage of Terminal Oxidants by Iron(III) Porphyrin Complexes. *J. Am. Chem. Soc.* **2018**, *140*, 5127−5137.

(23) Song, W. J.; Seo, M. S.; DeBeer George, S.; Ohta, T.; Song, R.; Kang, M.-J.; Tosha, T.; Kitagawa, T.; Solomon, E. I.; Nam, W. Synthesis, Characterization, and Reactivities of Manganese(V)-Oxo Porphyrin Complexes. *J. Am. Chem. Soc.* **2007**, *129*, 1268−1277.

(24) Groves, J. T.; Nemo, T. E. Epoxidation Reactions Catalyzed by Iron Porphyrins. Oxygen Transfer from Iodosylbenzene. *J. Am. Chem. Soc.* **1983**, *105*, 5786−5791.

(25) (a) Gupta, R.; Li, X.-X.; Cho, K.-B.; Guo, M.; Lee, Y.-M.; Wang, Y.; Fukuzumi, S.; Nam, W. Tunneling Effect That Changes the Reaction Pathway from Epoxidation to Hydroxylation in the Oxidation of Cyclohexene by a Compound I Model of Cytochrome P450. *J. Phys. Chem. Lett.* **2017**, *8*, 1557−1561. (b) Kim, S.; Cho, K.-B.; Lee, Y.-M.; Chen, J.; Fukuzumi, S.; Nam, W. Factors Controlling the Chemoselectivity in the Oxidation of Olefins by Nonheme Manganese(IV)-Oxo Complexes. *J. Am. Chem. Soc.* **2016**, *138*, 10654−10633. (c) Kwon, Y. H.; Mai, B. K.; Lee, Y.-M.; Dhuri, S. N.; Mandal, D.; Cho, K.-B.; Kim, Y.; Shaik, S.; Nam, W. Determination of Spin Inversion Probability, H.Tunneling Correction, and Regioselectivity in the Two-State Reactivity of Nonheme Iron(IV)-Oxo Complexes. *J. Phys. Chem. Lett.* **2015**, *6*, 1472−1476. (d) Hyun, M. Y.; Jo, Y. D.; Lee, J. H.; Lee, H. G.; Park, H. M.; Hwang, I. H.; Kim, K. B.; Lee, S. J.; Kim, C. Remarkable Solvent, Porphyrin Ligand, and Substrate Effects on Participation of Multiple Active Oxidants in Manganese(III) Porphyrin Catalyzed Oxidation Reactions. *Chem.—Eur. J.* **2013**, *19*, 1810−1818.

(26) (a) Nam, W.; Lim, M. H.; Oh, S.-Y.; Lee, J. H.; Lee, H. J.; Woo, S. K.; Kim, C.; Shin, W. Remarkable Anionic Axial Ligand Effects of Iron(III) Porphyrin Complexes on the Catalytic Oxygenations of Hydrocarbons by H_2O_2 and the Formation of Oxoiron(IV) Porphyrin Intermediates by *m*-Chloroperoxybenzoic Acid. *Angew. Chem., Int. Ed.* **2000**, *39*, 3646−3649. (b) Nam, W.; Oh, S.-Y.; Lim, M. H.; Choi, M.-H.; Han, S.-Y.; Jhon, G.-J. Temperature Effect on the Epoxidation of Olefins by an Iron(III) Porphyrin Complex and tert-Alkyl Hydroperoxides. *Chem. Commun.* **2000**, 1787−1788. (c) Nam, W.; Jin, S. W.; Lim, M. H.; Ryu, J. Y.; Kim, C. Anionic Ligand Effect on the Nature of Epoxidizing Intermediates in Iron Porphyrin Complex-Catalyzed Epoxidation Reactions. *Inorg. Chem.* **2002**, *41*, 3647−3652.

DOI: 10.1021/acs.inorgchem.8b01426
Inorg. Chem. XXXX, XXX, XXX−XXX

(27) (a) Garrison, J. M.; Ostovic, D.; Bruice, T. C. Is a Linear Relationship between the Free Energies of Activation and One-Electron Oxidation Potential Evidence for One-Electron Transfer Being Rate Determining? Intermediates in the Epoxidation of Alkenes by Cytochrome P-450 Models. 4. Epoxidation of a Series of Alkenes by Oxo(*meso*-tetrakis(2,6-dibromophenyl)porphinato)-Chromium-(V). *J. Am. Chem. Soc.* **1989**, *111*, 4960−4966. (b) Groves, J. T.; Watanabe, Y. On the Mechanism of Olefin Epoxidation by Oxo-Iron Porphyrins. Direct Observation of an Intermediate. *J. Am. Chem. Soc.* **1986**, *108*, 507−508.
(28) Armarego, W. L. F.; Chai, C. L. L. *Purification of Laboratory Chemicals*, 6th Edition; Pergamon Press: Oxford, U.K., 2009.
(29) Tenderholt, A.; Hedman, B.; Hodgson, K. O. In *X-ray Absorption Fine Structure—XAFS13*; Hedman, B., Pianetta, P., Eds.; AIP Conference Proceedings, Vol. *882*; American Institute of Physics: College Park, MD, 2007; p 105.
(30) Zabinsky, S. I.; Rehr, J. J.; Ankudinov, A.; Albers, R. C.; Eller, M. J. Multiple-Scattering Calculations of X-ray-Absorption Spectra. *Phys. Rev. B: Condens. Matter Mater. Phys.* **1995**, *52*, 2995−3009.
(31) Mustre de Leon, J.; Rehr, J. J.; Zabinsky, S. I.; Albers, R. C. Ab Initio Curved-Wave X-ray Absorption Fine Structure. *Phys. Rev. B: Condens. Matter Mater. Phys.* **1991**, *44*, 4146−4155.
(32) Rehr, J. J.; Mustre de Leon, J.; Zabinsky, S. I.; Albers, R. C. Theoretical X-ray Absorption Fine Structure Standards. *J. Am. Chem. Soc.* **1991**, *113*, 5135−5140.
(33) George, G. N. *EXAFSPAK and EDG-FIT*; Stanford Synchrotron Radiation Laboratory, Stanford Linear Accelerator Center: Stanford, CA, 2000.
(34) Neese, F. *ORCA: An Ab Initio, DFT and Semiempirical SCF-MO Package*, Version 3.0.1; Max Planck Institute for Chemical Energy Conversion: Stuttgart, Germany, 2013.
(35) Becke, A. D. Density-Functional Exchange-Energy Approximation with Correct Asymptotic Behavior. *Phys. Rev. A: At., Mol., Opt. Phys.* **1988**, *38*, 3098−3100.
(36) Perdew, J. P.; Burke, K.; Wang, Y. Generalized Gradient Approximation for the Exchange-Correlation Hole of a Many-Electron System. *Phys. Rev. B: Condens. Matter Mater. Phys.* **1996**, *54*, 16533−16539.
(37) Schaefer, A.; Horn, H.; Ahlrichs, R. Fully Optimized Contracted Gaussian Basis Sets for Atoms Li to Kr. *J. Chem. Phys.* **1992**, *97*, 2571−2577.
(38) Schaefer, A.; Huber, C.; Ahlrichs, R. Fully Optimized Contracted Gaussian Basis Sets of Triple Zeta Valence Quality for Atoms Li to Kr. *J. Chem. Phys.* **1994**, *100*, 5829−5835.
(39) Weigend, F.; Ahlrichs, R. Balanced Basis Sets of Split Valence, Triple Zeta Valence and Quadruple Zeta Valence Quality for H to Rn: Design and Assessment of Accuracy. *Phys. Chem. Chem. Phys.* **2005**, *7*, 3297−3305.

DOI: 10.1021/acs.inorgchem.8b01426
Inorg. Chem. XXXX, XXX, XXX−XXX